A Gaussian Process-Based Receding Horizon Adaptive Control Strategy for Energy-Efficient Exploration of Spatiotemporally Varying Environments, with Application to Airborne Wind Energy Systems

Ayaz Siddiqui[1], Ben Haydon[2], and Chris Vermillion[3]

***Abstract*— Numerous mobile systems face the challenge of simultaneously exploring and exploiting a stochastic, spatiotemporally varying environment. The present work focuses on the development of an adaptive control strategy that fuses Gaussian process modeling and receding horizon control to ideally manage the tradeoff between *exploration* (i.e., maintaining an adequate map of the resource) and *exploitation* (i.e., carrying out a mission, which consists in this work of harvesting the resource). The use of a receding horizon formulation aids in the consideration of limited mobility, which is characteristic of dynamical systems. In this work, we focus on an airborne wind energy (AWE) system as a case study, where the system can vary its elevation angle (tether angle relative to the ground, which trades off higher efficiency with higher-altitude operation) and flight path parameters in order to maximize power output in a wind environment that is changing in space and time. We demonstrate the effectiveness of the proposed approach through a data-driven study on a rigid wing-based AWE system.**

I. Introduction

In recent years, many commercial and research institutions have been working in the area of airborne wind energy (AWE) systems [1]. These systems replace conventional towers with tethers and a lifting body to reach altitudes that are inaccessible with traditional wind turbines, and can execute high-speed crosswind flight to dramatically enhance power output (see [2], [3], [4], [5], [6]). These systems can either generate energy via on-board rotors or through cyclic spooling motion, where tether is reeled out under high tension, in crosswind flight, and reeled in under low tension, often with crosswind flight suspended. In either case, the majority of the literature on AWE systems is focused on optimization of the crosswind path in deterministic wind shear profiles and robust control, often in the presence of turbulence (see [7], [8], [9], [10], [11], [12]). The authors of [8] use iterative learning to optimize the width and height of the crosswind path while operating at a constant mean altitude in realistic flow, whereas the authors of [9] demonstrate robust path tracking in artificially generated random wind conditions. Similarly, the authors of [10] provide a means to maximize power generation in the presence of a deterministic mean profile superimposed with random turbulence. The authors of [13] perform an offline optimization of mean elevation angle and tether reel-out speeds as functions of wind speeds. However, optimization of mean elevation angle (consequently the operating altitude) in spatiotemporally varying, partially observable wind profiles is a problem that has not been addressed in the crosswind kite literature. This problem is particularly challenging in the case of partial observability, where the AWE system only has knowledge of the power output at its present location, for its present flight path parameters, thereby leading to a tradeoff between *exploration* (i.e., maintaining an accurate map of wind speed/power output as a function of location and flight path parameters) and *exploitation* (i.e., operating at the estimated optimal location and flight path parameters).

On the other hand, optimization of operating altitude in spatiotemporally varying, partially observable wind profiles has been researched in the context of lighter-than-air AWE systems that do not execute crosswind flight, like the Altaeros BAT [14], where Gaussian Process (GP) modeling and Bayesian optimization (BO) [15] has been utilized to maximize power generation (see [16], [17], [18]). The authors of [16] and [17] use GP-based BO to optimize altitude in realistic wind conditions, whereas the authors of [18] study the impact of different sensor configurations on performance using a persistence model for the wind profile.

At first glance, it may appear that the GP-based altitude optimization techniques that have been applied successfully in the case of non-crosswind systems represent a complete work that can be directly extended to the optimization of the elevation angle and flight path profiles of systems that execute crosswind flight, along with other mobile systems that operate in spatiotemporally varying environments. However, some critical and coupled limitations related to dimensionality of the problem and dynamic considerations preclude such a direct extension. Specifically, the aforementioned GP-based techniques require a database of all past measurements. While very old measurements can be purged without significant effect on performance (as in [16]), this still does not represent a tenable solution in a dynamic environment with great disparities in time scales, where measurements are collected at every (short) time step. Furthermore, computational requirements grow cubically with the number of past time steps for which data is saved. For the aforementioned non-crosswind applications, maintenance of

This work was supported by the US Department of Energy, under the award entitled "Device Design and Robust Period Motion Control of an Ocean Kite System for Hydrokinetic Energy Harvesting" (US Department of Energy Award No. DE-EE0008635).

[1]Ayaz Siddiqui is a PhD candidate at North Carolina State University asiddiq2@ncsu.edu.

[2]Ben Haydon is a PhD candidate at North Carolina State University brhaydon@ncsu.edu.

[3]Chris Vermillion is an Associate Professor in the Department of Mechanical and Aerospace Engineering at North Carolina State University, Raleigh, NC 27695, USA cvermil@ncsu.edu.

this database represented a computationally feasible strategy due to two unique features of the problem. First, a simple power curve could be used to express the power output only as a cubic function of the local wind speed (up to the rated wind speed). Because the local wind speed was the only determinant of power output, a very slow sampling rate, on the order of minutes, could be used for populating the GP model database. Secondly, the optimization involved only one decision variable – altitude. As soon as either of these features cease to exist in an application, the use of traditional GP techniques becomes infeasible for real-time implementation. For AWE systems that execute crosswind flight, power output is a complex function not only of wind speed but also of the kite's elevation angle and path geometry. As a result, effective adaptation algorithms require more adjustments (and therefore faster sampling periods) relative to the time scales associated with the wind. Furthermore, several control variables can be modified to affect power output, including elevation angle, tether length, and path parameters. An ideal adaptation algorithm should be able to be expanded in a computationally tractable way to address the full suite of control variables.

In this work, we develop a GP-based model predictive control (MPC) formulation that utilizes a Kalman filter representation to characterize the GP through a finite and fixed number of state variables. The use of a finite number of state variables, rather than a growing database, leads to real-time tractability and extendability to higher-dimensional problems. The MPC formulation allows for consideration of mobility constraints while also enabling the controller to look far enough into the future to properly consider the long-term implications of its exploration strategy. In this work, we optimize the elevation angle of an AWE system with on-board power generation, which executes crosswind motions. We demonstrate the efficacy of the proposed approach on this application, in addition to performing a parametric trade study to quantify the impact of control design parameters on performance.

II. Preliminaries

In this section, we provide necessary preliminary information regarding crosswind AWE systems, GP regression, Kalman filtering, and spectral factorization of random processes.

A. Crosswind Kite System

The crosswind AWE system considered in this work consists of a kite connected to the base station via a single flexible tether, as shown in Fig. 1. The system is designed to execute power-augmenting crosswind motion (high-speed figure-8 or circular patterns perpendicular to the prevailing flow) to increase the apparent flow, thereby substantially increasing power generation [19].

In general, AWE systems can generate power in either of two ways:

1) *On-board power generation*, where turbine(s) attached to the kite transmit energy to a base station via a conductive tether [3], [4].

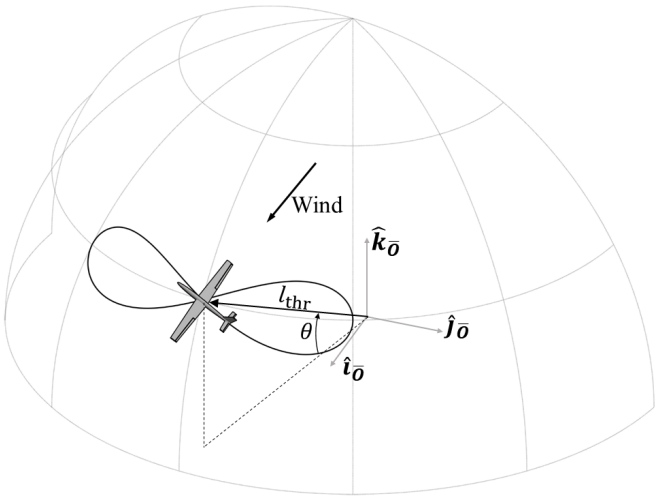

Fig. 1: Schematic of kite executing crosswind flight on a figure-8 path with mean elevation angle, θ, and tether length, l_{thr}. Here the wind vector is aligned with the $\hat{i}_{\bar{O}}$ unit axis.

2) *Ground based systems*, such as those developed by [5], [6], where a motor/generator winch system at the ground spools out tether under high tension and spools in tether under low tension, resulting in net positive energy generation.

The case study in this paper focuses on on-board power generation.

B. Gaussian Process Modeling

Gaussian process (GP) modeling is a machine learning technique that is used to infer a latent function $f(\cdot)$ from the data $\mathcal{D} = \{(\mathbf{p}_1, y_1), \ldots, (\mathbf{p}_n, y_n)\}$, where $\mathcal{D}$ is drawn from a noisy process,

$$y_i = f(\mathbf{p}) + \varepsilon. \tag{1}$$

Here, $\mathbf{p}_i \in \mathbb{R}^d$ are input vectors, $y_i \in \mathbb{R}$ are observations or outputs, and $\varepsilon \sim \mathcal{N}(0, \sigma_n^2)$ is zero-mean Gaussian noise with variance σ_n^2.

A GP model is fully defined by a mean function $m(\mathbf{p})$ and a covariance function $k(\mathbf{p}, \mathbf{p}')$, and is expressed as follows:

$$\begin{aligned} f(\mathbf{p}) &\sim \mathcal{GP}\big(m(\mathbf{p}), k(\mathbf{p}, \mathbf{p}')\big) \\ \text{where: } m(\mathbf{p}) &= \mathbb{E}[f(\mathbf{p})] \\ k(\mathbf{p}, \mathbf{p}') &= \mathbb{E}[(f(\mathbf{p}) - m(\mathbf{p}))(f(\mathbf{p}') - m(\mathbf{p}'))]. \end{aligned} \tag{2}$$

Given a data set of previously tested points denoted by $\{\mathbf{p}_\mathcal{D} = \mathbf{p}_{1:n}, \mathbf{y}_\mathcal{D} = y_{1:n}\}$, prediction mean and variance for any candidate point $\mathbf{p}_*$, are given by

$$\bar{f}(\mathbf{p}_*) = k(\mathbf{p}_*, \mathbf{p}_\mathcal{D}) K_\mathcal{D}^{-1} \mathbf{y}_\mathcal{D} \tag{3}$$

$$\mathbb{V}[f(\mathbf{p}_*)] = k(\mathbf{p}_*, \mathbf{p}_*) - k(\mathbf{p}_*, \mathbf{p}_\mathcal{D}) K_\mathcal{D}^{-1} k(\mathbf{p}_\mathcal{D}, \mathbf{p}_*), \tag{4}$$

where $K_\mathcal{D}$ is the covariance matrix between all input vectors plus the measurement noise, i.e. $K_\mathcal{D} = k(\mathbf{p}_\mathcal{D}, \mathbf{p}_\mathcal{D}) + \sigma_n^2 I$. Because of the matrix inversion in both Eqn. (3) and Eqn. (4), the method scales as $O(n^3)$. In real-time control applications, where measurements are collected at each time step, keeping all the past measurements in memory and inverting $K_\mathcal{D}$

in a relatively short amount of time becomes intractable. Thus, applying GP modeling directly to real-time control applications is generally not feasible.

C. Kalman Filtering for Discrete-Time Linear System

Consider the following system:

$$\begin{aligned} s_{k+1} &= As_k + w_k \\ y_k &= C_k s_k + v_k \end{aligned} \tag{5}$$

where, at each time step k, $s_k \in \mathbb{R}^n$ is the state vector, $y_k \in \mathbb{R}^m$ is the output vector, $w_k \in \mathbb{R}^n$ and $v_k \in \mathbb{R}^m$ are i.i.d. zero-mean Gaussian random vectors with covariance matrices $Q \geq 0$ and $R > 0$, respectively. $A \in \mathbb{R}^{n\times n}$ is the state matrix and $C_k \in \mathbb{R}^{m\times n}$ is the time-varying output matrix. Typically, both the process and measurement noise are assumed to be uncorrelated, i.e., $\mathbb{E}[w_k^T v_h] = 0 \; \forall_{k,h}$.

The Kalman filter [20] applied to the system in Eqn. (5) is described by the following recursive equations:

$$\hat{s}_{k+1|k} = A\hat{s}_{k|k} \tag{6a}$$
$$\Sigma_{k+1|k} = A\Sigma_{k|k}A^T + Q \tag{6b}$$
$$L_{k+1} = \Sigma_{k+1|k}C_k^T(C_k\Sigma_{k+1|k}C_k^T + R)^{-1} \tag{6c}$$
$$\hat{s}_{k+1|k+1} = \hat{s}_{k+1|k} + L_{k+1}(y_{k+1} - C_k\hat{s}_{k+1|k}) \tag{6d}$$
$$\Sigma_{k+1|k+1} = \Sigma_{k+1|k} - L_{k+1}C_k\Sigma_{k+1|k} \tag{6e}$$

where $\hat{s}_{k|k}$ and $\Sigma_{k|k}$ represent the filtered estimate of the state and the posterior error covariance, respectively; $\hat{s}_{k+1|k}$ and $\Sigma_{k+1|k}$ represent the (one step) predicted state estimate and error covariance, respectively; and L_{k+1} is the Kalman gain.

D. Spectral factorization of random processes

Consider a stationary random process $f(t)$ with covariance $h(\tau)$. From the Wiener-Khinchin theorem [21], it is known that the power spectral density (PSD) of the process is equal to the Fourier transform of its covariance, i.e.,

$$S(\omega) \triangleq \mathscr{F}[h(\tau)](\omega) \tag{7}$$

Moreover, in the particular case when $S = S_r$ is rational of order $2r$, using spectral factorization [21], its PSD can be rewritten as $S_r = W(\mathbf{i}\omega)W(-\mathbf{i}\omega)$ with

$$W(\mathbf{i}\omega) = \frac{b_{r-1}(\mathbf{i}\omega)^{r-1} + b_{r-2}(\mathbf{i}\omega)^{r-2} + \ldots + b_0}{(\mathbf{i}\omega)^r + a_{r-1}(\mathbf{i}\omega)^{r-1} + \ldots + a_0} \tag{8}$$

Finally, from realization theory, rational transfer functions of the form of Eqn. (8) can be expressed as a continuous-time state space representation [22] given by

$$\begin{aligned} \dot{s}_t &= Fs_t + Gw_t \\ z_t &= Hs_t. \end{aligned} \tag{9}$$

III. Kalman Filtering of Gaussian Process

To overcome the memory limitations of iterative GP (specifically, the requirement that the GP model maintain a complete database of all past measurements), the authors of [23] developed a state-space representation of Gaussian processes. This algorithm allows for recursive calculation of the minimum variance prediction of a spatiotemporally varying, partially observable process at time step k over arbitrary spatial locations, under the following assumptions:

1) The process covariance is separable in space and time.
2) The temporal kernel is stationary and has a rational power spectral density.
3) Measurements are collected over a finite set of spatial locations.

A. Measurement space

Let $\mathbf{X}$ be the set of all spatial locations. The measurement space is a set of spatial locations containing M points where measurements can be collected and is defined as

$$\mathbf{X}_\mathrm{M} \triangleq \{\mathbf{x}_1, ..., \mathbf{x}_M | \mathbf{x}_i \in \mathbf{X}\}$$

Measurements are collected at discrete time instants $t_k = kT$, where T denotes the sampling time, from a time-varying subset of the measurement space, namely $\mathcal{M}(k) \subseteq \mathbf{X}_\mathrm{M}$. Figure 2 shows an illustrative representation of the measurement collection and prediction process.

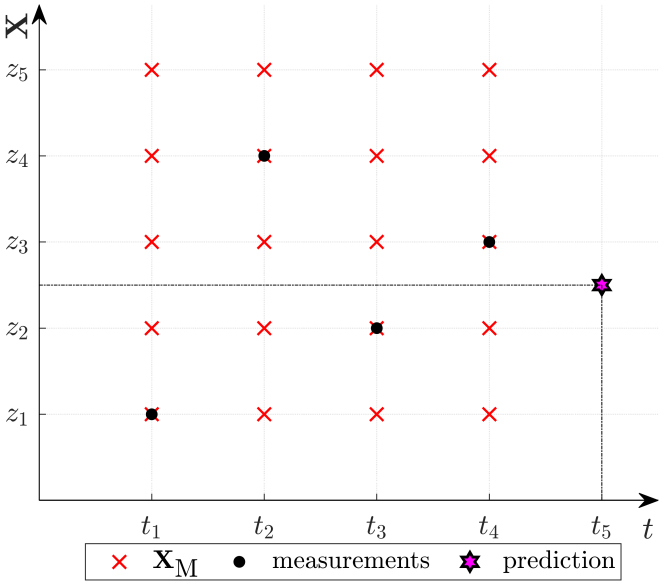

Fig. 2: Illustrative representation of the measurement collection and prediction process: the x-axis represents discrete time instants while the y-axis represents the spatial domain $\mathbf{X}$. Red crosses highlight all the measurements locations contained in $\mathbf{X}_\mathrm{M}$. Black circles represent the locations $\mathcal{M}(k)$ where measurements are actually collected. The magenta star represents a generic prediction location.

B. Covariance kernel properties

The covariance kernel, $k(\mathbf{p}, \mathbf{p}')$, of the GP is chosen such that it is separable in space and time as follows:

$$k(\mathbf{p}, \mathbf{p}') = g(\mathbf{x}, \mathbf{x}')h(t, t'), \tag{10}$$

where $\mathbf{p} = [\mathbf{x}\ t]^T$, $g(\mathbf{x}, \mathbf{x}')$ is the spatial covariance, and $h(t, t')$ is the temporal covariance. In addition, the temporal kernel is stationary and its power spectral density $S_r = W(\mathbf{i}\omega)W(-\mathbf{i}\omega)$ is a rational function of order $2r$, where $W(\mathbf{i}\omega)$ can be written as Eqn. (8). It is worth noting that,

in cases when the PSD $S(\omega)$ of $h(t,t')$ is not rational it is always possible to build a rational PSD which approximates the true one. Different approximating methods can be used, e.g., Taylor series expansion or Pade approximation.

C. Kalman regression on $\mathbf{X}_\mathrm{M}$

Assuming that the GP covariance adheres to the form given in Eqn. (10) and measurements are collected periodically at every $t_k = kT$ at $\mathcal{M}(k)$ spatial locations, then as per [23], the process estimate, $\hat{\mathbf{f}}_k \triangleq [f(\mathbf{x}_1,t_k),\ldots,f(\mathbf{x}_M,t_k)]$, and corresponding error covariance, $\Sigma^{\mathbf{f}}$, are given by

$$\hat{\mathbf{f}}_k = K_s^{1/2}\mathbf{H}\hat{\mathbf{s}}_k \tag{11}$$
$$\Sigma^{\mathbf{f}} = K_s^{1/2}\mathbf{H}\Sigma_k\mathbf{H}^T K_s^{1/2} \tag{12}$$

where $\mathbf{H} \triangleq blkdiag(H,\ldots,H)$, $K_s \triangleq g(\mathbf{X}_\mathrm{M},\mathbf{X}_\mathrm{M})$ is the spatial covariance matrix, $\hat{\mathbf{s}}_k$ and Σ_k are the outputs of the time-varying Kalman filter of Eqn. (6) applied to the discrete-time system of Eqn. (5) with matrices (A, C_k, Q, R), where $A \triangleq blkdiag(\bar{F},\ldots,\bar{F})$, $Q \triangleq blkdiag(\bar{Q},\ldots,\bar{Q})$, $\bar{F}$ and $\bar{Q}$ are given by

$$\bar{F} = e^{FT}, \quad \bar{Q} = \int_0^T (e^{F\tau})GG^T(e^{F\tau})^T\, d\tau \tag{13}$$

and where the triplet (F,G,H) is calculated as per Section II-D, $R \triangleq \sigma_n^2 I$, and $C_k \triangleq I_k K_s^{1/2}\mathbf{H}$ with $I_k \in \{0,1\}^{M_k\times M}$ being the indicator matrix selecting the locations contained in $\mathcal{M}(k)$.

D. Kalman regression on $\mathbf{X}$

Section III-C showed how to build an estimate $\hat{\mathbf{f}}_k$ of the process over the observable finite-dimensional set $\mathbf{X}_\mathrm{M}$. This section summarizes the procedure for obtaining a minimum variance estimate at any spatial location as detailed in [23].

Consider any spatial location $\mathbf{x} \in \mathbf{X}$. At time step t_k, the minimum variance process estimate and the posterior variance at $\mathbf{x}$ are given by

$$\begin{aligned}\hat{f}(\mathbf{x},t_k) &= \Psi\hat{\mathbf{f}}_k \\ \mathbb{V}(\hat{f}(\mathbf{x},t_k)) &= g(\mathbf{x},\mathbf{x}) - \Psi(K_s - \Sigma^{\mathbf{f}})\Psi^T\end{aligned} \tag{14}$$

where $\Psi = g(\mathbf{x},\mathbf{X}_\mathrm{M})K_s^{-1}$. The above results state that the outputs of the Kalman filter capture all the necessary information to estimate the process over the entire domain $\mathbf{X}$.

IV. Medium-Fidelity AWE System Power Generation Model

Turing to our AWE system case study, this section presents a medium-fidelity model for characterizing the power output of an airborne kite executing cross-current motions, using on-board power generation.

A. External loads

The net external force vector acting on the the kite is the sum of forces due to gravity, hydrodynamic lift and drag, turbine drag, and tether tension, given as follows:

$$\begin{aligned}\vec{F}_{\text{net}} =& \vec{F}_{\text{grav}} + \vec{F}_{\text{lift}} + \vec{F}_{\text{drag}} + \vec{F}_{\text{turb}} + \vec{F}_{\text{thr}} \\ =& -mg\hat{k}_{\bar{O}} + A_r qC_L\vec{u}_L + A_r qC_D\vec{u}_D + \\ & A_t qC_{D,t}\vec{u}_D + F_{thr}\hat{k}_{\bar{T}}\end{aligned}$$

Here, m is the kite mass, g is the gravitational acceleration, A_r is the kite reference area, A_t is the turbine area, F_{thr} is the force exerted by the tether on the kite, and $\hat{k}_{\bar{T}}$ is the radial unit vector which connects the center of the sphere to the kite. The variables C_L and C_D denote the lift and drag coefficients of the kite whereas $C_{D,t}$ is the turbine drag coefficient. The resulting fluid dynamic force depends on the dynamic pressure, which in turn is dependent on the apparent wind at the kite, and is given by:

$$\begin{aligned}q &= \frac{1}{2}\rho\|\vec{v}_a\|^2 \\ &= \frac{1}{2}\rho\|\vec{v}_w - \vec{v}_k\|^2,\end{aligned} \tag{15}$$

where $\vec{v}_w$ is the wind velocity and $\vec{v}_k$ is the kite velocity. Lastly, $\vec{u}_D$ and $\vec{u}_L$ are unit vectors pointing in the direction of the drag and lift force of the kite, where $\vec{u}_D$ acts in the direction parallel to the apparent flow $\vec{v}_a$, while $\vec{u}_L$ acts perpendicular to $\vec{u}_D$ and in the longitudinal plane of the kite.

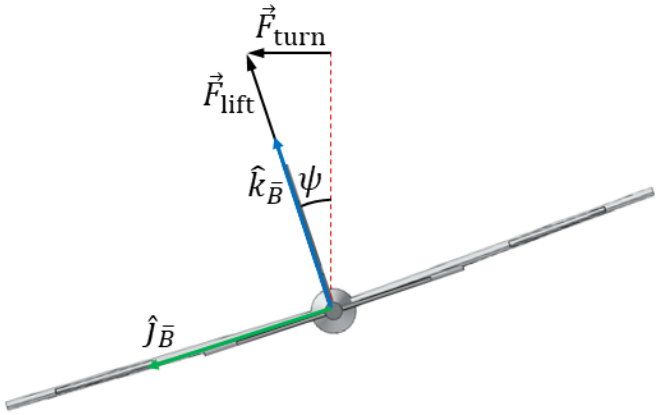

Fig. 3: Schematic of back view of kite showing the transverse and vertical axes, roll angle, lift force and, the turning lift force

B. Path radius of curvature

Given path parameters, a and b, and the path mean elevation angle, θ, the path azimuth and elevation are given by

$$\begin{aligned}\phi_p(s) &= \frac{a\sin(s)}{1+\left(\frac{a}{b}\cos(s)\right)^2} \\ \theta_p(s) &= \frac{\frac{a^2}{b^2}\sin(s)\cos(s)}{1+\left(\frac{a}{b}\cos(s)\right)^2} + \theta\end{aligned} \tag{16}$$

where s is a path parameter that varies from 0 to 2π, describing a particular location on the path. The position of the path in the ground frame is calculated using standard spherical to Cartesian conversion, as follows:

$$\begin{aligned} x_p(s) &= l_{\text{thr}} \cos(\phi_p(s)) \cos(\theta_p(s)) \\ y_p(s) &= l_{\text{thr}} \sin(\phi_p(s)) \cos(\theta_p(s)) \\ z_p(s) &= l_{\text{thr}} \sin(\theta_p(s)) \end{aligned} \tag{17}$$

We then calculate the radius of curvature by

$$R_{\text{curv}} = \frac{(\dot{x}_p^2 + \dot{y}_p^2 + \dot{z}_p^2)^{3/2}}{\sqrt{D}} \quad \text{where} \tag{18}$$
$$D = (\ddot{z}_p\dot{y}_p - \ddot{y}_p\dot{z}_p)^2 + (\ddot{x}_p\dot{z}_p - \ddot{z}_p\dot{x}_p)^2 + (\ddot{y}_p\dot{x}_p - \ddot{x}_p\dot{y}_p)^2$$

where $\dot{x}_p$, $\dot{y}_p$, $\dot{z}_p$, $\ddot{x}_p$, $\ddot{y}_p$, and $\ddot{z}_p$ denote first and second derivatives with respect to the path parameter s.

C. Tangent roll angle dynamics

As illustrated in Fig. 3, the kite uses roll control to re-vector its lift in order to stay on the target path (or return to the target path, as necessary). To characterize the dynamics associated with this motion, we consider a coordinate system $(\hat{i}_{\bar{B}}, \hat{j}_{\bar{B}}, \hat{k}_{\bar{B}})$ attached to the kite, where $\hat{i}_{\bar{B}}$ is along the kite longitudinal axis pointing forward, $\hat{j}_{\bar{B}}$ lies along the kite transverse axis pointing to the left wingtip, and $\hat{k}_{\bar{B}}$ lies along the kite vertical axis pointing upward.

We assume that a secondary controller keeps the kite's velocity vector aligned tangential to the path and in the tangent plane, spanning (ϕ_p, θ_p), tangent to the sphere centered at the ground station and with the radius equal to the tether length. In fact, our prior work in [24] describes and validates such a controller. In particular, by altering the tangent roll angle, defined by ψ in Fig. 3 (which represents the angle between the kite's lateral axis and the sphere on which the kite is flying), a component of the kite's lift vector points in a leftward or rightward direction relative to the sphere on which the kite is flying. This allows the kite to navigate itself back to the target path. The corresponding component of lifting force in the plane tangent to the sphere on which the kite is flying is given by

$$\vec{F}_{\text{turn}} = \vec{F}_{\text{lift}} \sin(\psi). \tag{19}$$

The required centripetal force for the kite to follow the prescribed path can be calculated by

$$\vec{F}_{\text{cent}} = \frac{m\|\vec{v}_k\|^2}{R_{\text{curv}}} \tag{20}$$

and acts in a direction perpendicular to the path. Lastly, we compute the required roll angle to follow the path and achievable steady-state kite speed by numerically solving the following system of equations at each location along the path:

$$\vec{F}_{\text{net}} \cdot \hat{i}_{\bar{T}} = 0 \tag{21}$$
$$\vec{F}_{\text{turn}} - \vec{F}_{\text{cent}} = 0 \tag{22}$$
$$F_{thr} + (\vec{F}_{\text{grav}} + \vec{F}_{\text{lift}} + \vec{F}_{\text{drag}}) \cdot \hat{k}_{\bar{T}} = 0 \tag{23}$$

The net power generated over one figure-8 lap is given by

$$P_{\text{lap}} = \int_0^{2\pi} \frac{1}{2} C_p \rho (-v_a(s) \cdot \hat{i}_{\bar{B}})^3 \pi A_t \, \text{ds} \tag{24}$$

where C_p is the power coefficient.

V. Adaptive Control Strategy

The goal of the presented adaptive control strategy is to optimize the mean elevation angle of the AWE kite system to maximize power generation of the kite in a partially observable and spatiotemporally varying wind shear profile. Therefore, the control strategy must achieve a balance between learning more about the environment over the control space (exploration) and selecting a mean elevation angle that is deemed optimal based on the collected data (exploitation), while accounting for future evolution of the wind shear profile. Model predictive control (MPC) with a Kalman filter-based GP model is used for this purpose.

A. MPC setup

The goal of MPC is to use a model of the process to predict the future evolution of the system and compute control actions by optimizing a cost function that depends on these predictions [25]. In performing this optimization, MPC can explicitly consider hard constraints on both the control signal and the system states.

The overall goal of the adaptive controller can be summarized by the following optimization problem:

$$\begin{aligned} \boldsymbol{\theta}^*_{sp}(k) = \ & \arg\max_{\theta} J(\boldsymbol{\theta}_{sp}(k)) \\ \text{Subject to: } & |\theta(i|k) - \theta(i-1|k)| \leq \theta_{lim} \\ & \theta(i|k) \in [\theta_{min}, \theta_{max}] \ \forall \ i \end{aligned} \tag{25}$$

where

$$J(\boldsymbol{\theta}_{sp}(k)) = \sum_{i=k}^{k+P-1} \left(J_{exploit}(\theta_{sp}(k)) + 2^{\beta} J_{explore}(\theta_{sp}(k)) \right)$$

Here, P is the MPC prediction horizon, β is the weighing constant that balances exploration versus exploitation, $[\theta_{min}, \theta_{max}]$ is the set that spans the allowable mean elevation angles, and θ_{lim} is a rate limitation constant used to limit the change in the mean elevation over one time step. The vector $\boldsymbol{\theta}_{sp}$ corresponds to the mean elevation angle trajectory vector over the prediction horizon, given as

$$\boldsymbol{\theta}_{sp}(k) = [\theta_{sp}(k|k) \ldots \theta_{sp}(k|k+P-1)]^T \tag{26}$$

As is typical with MPC, the first term in the optimized control input trajectory represents the commanded control input at step k. In this case, the commanded control input is the mean elevation angle setpoint, given as

$$\theta_{sp} = \theta^*_{sp}(k|k) \tag{27}$$

The exploration and exploitation terms in the reward function are given by

$$J_{explore}(\theta_{sp}(k)) = \left(\mathbb{V}(\hat{f}(z_{sp}(k), t_k)) \right)^{3/2} \tag{28}$$
$$J_{exploit}(\theta_{sp}(k)) = \left(\hat{f}(z_{sp}(k), t_k) \cos(\theta_{sp}(k)) \right)^3 \tag{29}$$

where $J_{exploit}(\theta_{sp}(k))$ is a surrogate for expected power generation subject to cosine losses [26], $\hat{f}(\theta_{sp}(k), t_k)$ and $\mathbb{V}(\hat{f}(z_{sp}(k), t_k))$ are prediction mean and variance of the flow speed at time step t_k calculated as per Eqn. (14) at altitude, $z_{sp}(k) = l_{\text{thr}} \sin(\theta_{sp}(k))$, where l_{thr} is the tether length.

VI. Results

A. Synthetic wind profile and statistical characterization for GP model

To characterize the proposed adaptive control technique in a realistic wind environment, one year of wind data obtained from a 900 MHz Doppler wind profiler deployed in Lewes, Delaware [27] was used to identify hyperparameters of a GP model. Using a process described in [28], hyperparameters identified from this (relatively limited) data set were used to generate a large synthetic data set, which was in turn used for the validation of the proposed control approach.

For the GP model, where the spatial variable is altitude (z), the mean function was chosen to be a standard power law model, whereas the covariance kernel was selected as a squared exponential kernel:

$$m(z) = v_0 \left(\frac{z}{z_0}\right)^b = az^b, \tag{30}$$

$$g(z, z') = \sigma^2 \exp\left(-\frac{(z-z')^2}{2l_z^2}\right), \tag{31}$$

$$h(t, t') = \exp\left(-\frac{(t-t')^2}{2l_t^2}\right) \tag{32}$$

where σ, l_z, and l_t are the hyperparameters of the kernel. Specifically, σ^2 is the signal variance, which characterizes the expected deviation (squared) of a performance measurement from the mean, l_z and l_t are the length scales of the system that characterize how quickly the wind speed changes with respect to altitude, z, and time, t, respectively. The variable b is the power law exponent and v_0 is a reference wind speed at z_0, a reference altitude. The two parameters v_0 and z_0^b can be combined into a single coefficient denoted by a. The values of the hyperparameters were chosen to maximize the log marginal likelihood over 100 evaluations of the model with respect to the training data, which were calculated as follows:

$$\begin{aligned} -\log(p(\mathbf{y}|x)) =& \frac{1}{2}\mathbf{y}^T K(x,x)^{-1}\mathbf{y} \\ &+ \frac{1}{2} log|K(x,x)| + \frac{N}{2}\log 2\pi \end{aligned} \tag{33}$$

where N is the number of training points, $K(x, x)$ is the covariance matrix evaluated at all training points, $|\cdot|$ refers to the determinant, and $\mathbf{y}$ is the data collected at each training point. Using this methodology, the hyperparameters of the training data were identified as:

$$\begin{aligned} l_t = 22 \text{ min},\ l_z = 270 \text{ m},\ \sigma = 5.1 \text{ m/s}, \\ a = 3.77,\ b = 0.14 \end{aligned}$$

Figure 4 shows the synthetically generated wind shear profile at various time instances.

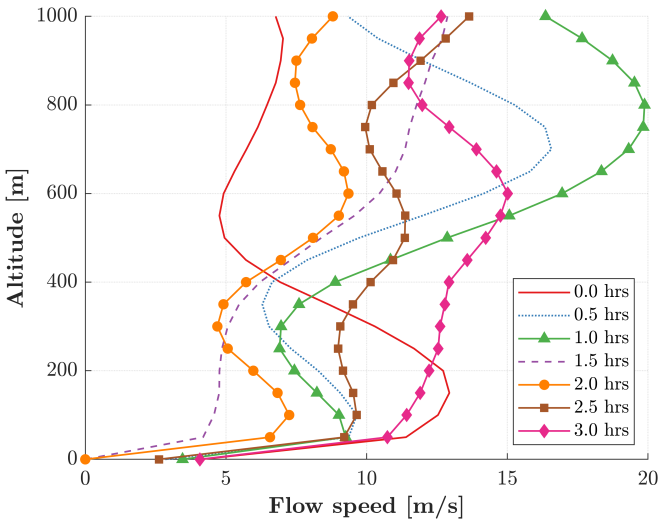

Fig. 4: Evolution of synthetically generated wind shear profile with time.

B. Kalman filter setup

To obtain the minimum variance prediction of wind speed using the recursive Kalman filtered GP, we first apply the Wiener-Khinchin theorem given in Eqn. (7) to the wind temporal kernel shown in Eqn. (32) to calculate its PSD, given by

$$S(\omega) = \sqrt{\frac{\pi}{\kappa}} \exp\left(-\frac{\omega^2}{4\kappa}\right) \tag{34}$$

where $\kappa = 1/2l_t^2$. Since the above PSD is not of rational order $2r$, we can think of $S(\omega)$ as a function of ω^2, and form a Taylor series approximation of $1/S(w)$ as follows:

$$\begin{aligned} \frac{1}{S(\omega)} =& \sqrt{\frac{\kappa}{\pi}} \exp\left(\frac{\omega^2}{4\kappa}\right) \\ \approx& \sqrt{\frac{\kappa}{\pi}}\left(1 + \frac{\omega^2}{4\kappa} + \frac{1}{2!}\frac{\omega^4}{(4\kappa)^2} + \ldots + \frac{1}{N!}\frac{\omega^{2N}}{(4\kappa)^N}\right) \\ =& \frac{1}{N!(4\kappa)^N}\sqrt{\frac{\kappa}{\pi}}\Big(N!(4\kappa)^N + N!(4\kappa)^{N-1}\omega^2 \\ &+ \frac{N!(4\kappa)^{N-2}}{2!}\omega^4 + \ldots + \omega^{2N}\Big) \end{aligned} \tag{35}$$

To simplify the results, we assume that N is even. The exact spectral density in Eqn. (34) can be approximated by the following spectral density:

$$S_r(\omega) = N!(4\kappa)^N \sqrt{\frac{\pi}{\kappa}}\left(\frac{1}{\sum_{n=0}^{N} \frac{N!(4\kappa)^{N-n}}{n!}\omega^{2n}}\right) \tag{36}$$

which has rational order $2r$ and can therefore be rewritten as $S_r = W(\mathbf{i}\omega)W(-\mathbf{i}\omega)$ and therefore can be expressed has continuous time state-space representation similar to Eqn. (9).

Lastly, the minimum variance prediction can be calculated using the steps detailed in Sections III-C and III-D. Figure 5 shows the comparison between computational time and percentage fit of the predictions obtained from the regression

using Kalman filtered GP ($N = 2$) to a batch GP calculated as

$$\text{Fit } [\%] = \left(1 - \frac{\|\bar{\mathbf{f}}_{\text{bgp}} - \hat{\mathbf{f}}_{\text{kfgp}}\|}{\|\bar{\mathbf{f}}_{\text{bgp}}\|}\right)100 \tag{37}$$

where $\bar{\mathbf{f}}_{\text{bgp}}$ and $\hat{\mathbf{f}}_{\text{kfgp}}$ denote the predictions obtained from batch GP and Kalman filtered GP, respectively. It can be seen that the percentage fit between the predictions obtained from the Kalman filtered GP and batch GP is over 95% over the entire duration of the simulation. On the other hand, the Kalman filtered GP maintains a constant computation time, in contrast with the increasing computation time for the batch GP.

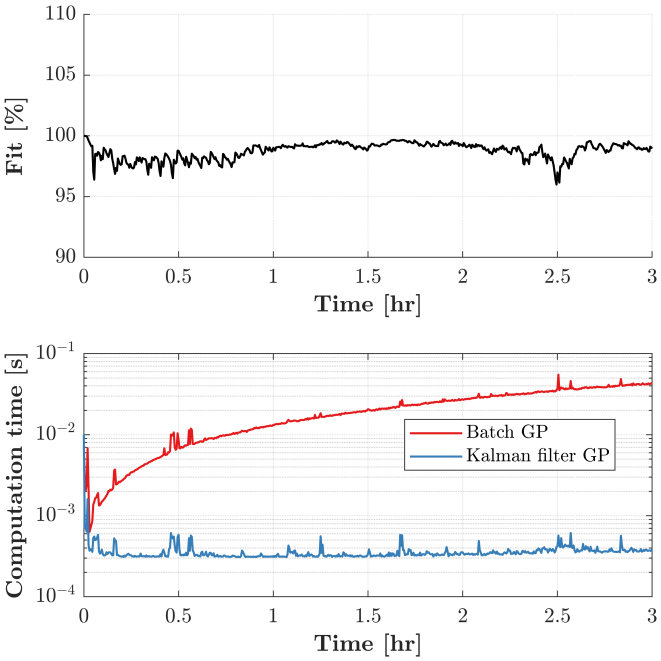

Fig. 5: Prediction and computational time comparison between batch GP and Kalman filtered GP.

C. Mean elevation angle control

To demonstrate the merits of the proposed adaptive controller, the system performance was compared across three different control strategies:

1) Offline optimized (Omniscient): In this strategy, we determine the optimum mean elevation that maximizes the surrogate for power generation given by Eqn. (29) by assuming a priori knowledge of the environment and no constraints on the change in elevation angle between time steps. Although this strategy is not implementable in real-time, it represents an upper bound on the potential of any control strategy.

2) Constant mean elevation (Baseline): In this strategy, the kite is operated at a constant mean elevation angle, which is calculated by taking the average of the mean elevation angles obtained from offline optimized strategy. This strategy is implementable in real time and represents a baseline control strategy.

3) MPC: This strategy uses the MPC control scheme of Eqn. (25) with an exploration versus exploitation weighing constant given by $\beta = 6$, rate limitation constant given by $\theta_{\text{lim}} = 5$ deg, and prediction horizon equal to 6 time steps.

Figure 6 shows the results obtained when using the aforementioned control strategies. The kite design is similar to the one used in [7] with the addition of a turbine with diameter equal to 0.44 m and power coefficient, $C_p = 0.5$. The ratio of average values of $J_{exploit}$ for MPC and baseline strategy at the end of simulation is equal to 2.19, showing a 119% improvement in performance.

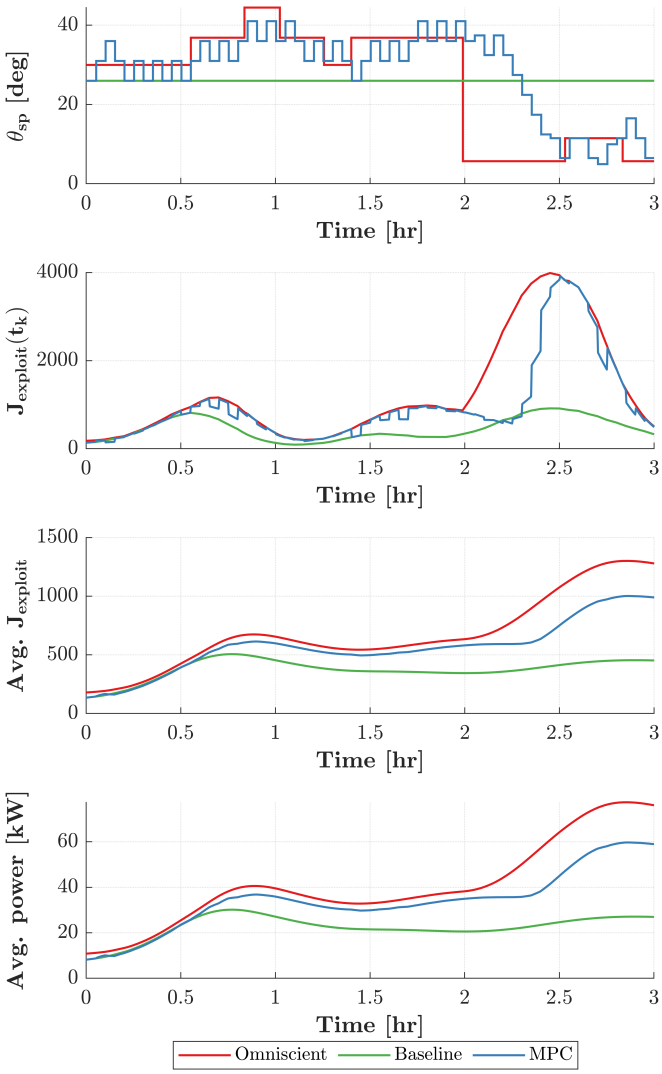

Fig. 6: Control strategy performance comparison.

D. Parameter sweep

To study the effect of mobility limitations and exploration vs. exploitation weighting on the MPC controller performance, we calculated the percentage improvement in performance over a range of θ_{lim} and β, for 500 synthetically generated wind profiles. Figure 7 demonstrates that for all the values of θ_{lim} and β, the MPC controller performs at least as well as the baseline strategy, and comparably with respect to the omniscient strategy. Also, not surprisingly,

when mobility restrictions are loosened through larger values of θ_{lim}, the MPC strategy is capable of achieving closer performance to the omniscient result with an appropriate exploration/exploitation balance.

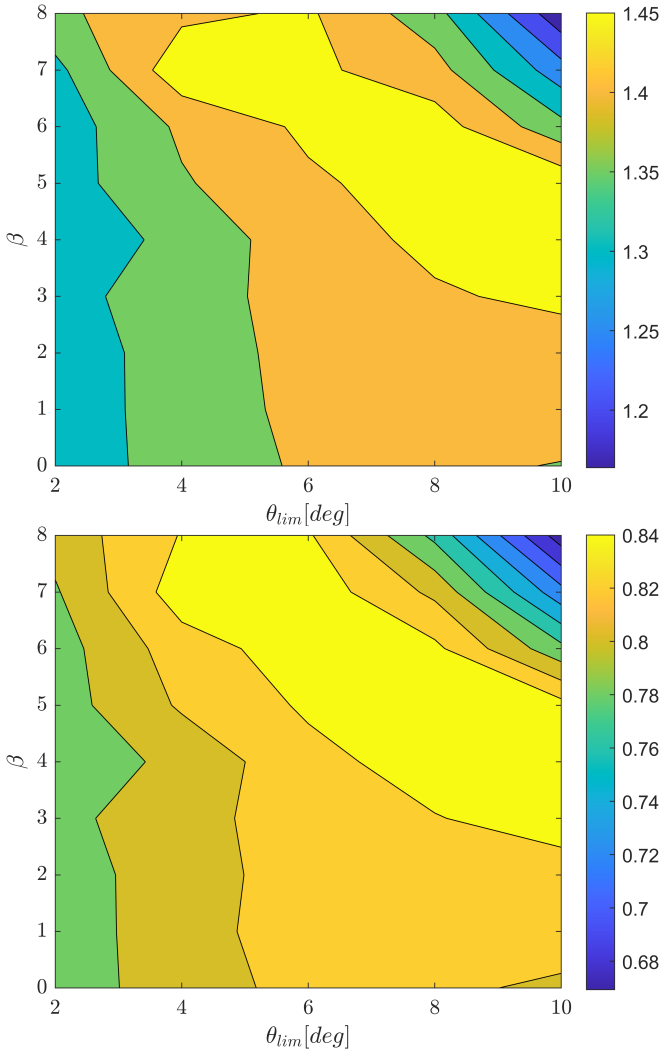

Fig. 7: Parameter sweep results for ratio of $J_{exploit}$ calculated for the MPC strategy to baseline strategy (top), and ratio of $J_{exploit}$ calculated for the MPC strategy and the omniscient controller (bottom) as a function of θ_{lim} and β

VII. Conclusion

In this paper, we presented a adaptive control strategy which fuses model predictive control (MPC) and Kalman filter-based Gaussian Process (GP) modeling to perform computationally tractable control in a partially observable, spatiotemporally varying environment. The proposed strategy was validated on an airborne wind energy (AWE) system, whereby a high-lift wing with on-board rotors executes power-augmenting crosswind flight. Results showed that the proposed strategy consistently outperforms a baseline strategy where the AWE system operates at a fixed elevation angle.

References

[1] A. Cherubini, A. Papini, R. Vertechy, and M. Fontana, "Airborne wind energy systems: A review of the technologies," *Renewable and Sustainable Energy Reviews*, vol. 51, pp. 1461–1476, 2015.

[2] M. Canale, L. Fagiano, and M. Milanese, "High altitude wind energy generation using controlled power kites," *IEEE Transactions on Control Systems Technology*, vol. 18, no. 2, pp. 279–293, 2009.

[3] Windlift. [Online]. Available: http://www.windlift.com/

[4] Kitemill. [Online]. Available: https://www.kitemill.com/

[5] KITEnrg. [Online]. Available: http://www.kitenergy.net/

[6] Ampyx Power. [Online]. Available: https://www.ampyxpower.com/

[7] G. Licitra, J. Koenemann, A. Bürger, P. Williams, R. Ruiterkamp, and M. Diehl, "Performance assessment of a rigid wing airborne wind energy pumping system," *Energy*, vol. 173, pp. 569–585, 2019.

[8] M. K. Cobb, K. Barton, H. Fathy, and C. Vermillion, "Iterative learning-based path optimization for repetitive path planning, with application to 3-d crosswind flight of airborne wind energy systems," *IEEE Transactions on Control Systems Technology*, 2019.

[9] P. Williams, B. Lansdorp, and W. Ockels, "Nonlinear control and estimation of a tethered kite in changing wind conditions," *Journal of guidance, control, and dynamics*, vol. 31, no. 3, pp. 793–799, 2008.

[10] M. Canale, L. Fagiano, and M. Milanese, "Power kites for wind energy generation [applications of control]," *IEEE Control Systems Magazine*, vol. 27, no. 6, pp. 25–38, 2007.

[11] M. Erhard and H. Strauch, "Control of towing kites for seagoing vessels," *IEEE Transactions on Control Systems Technology*, vol. 21, no. 5, pp. 1629–1640, 2012.

[12] A. U. Zgraggen, L. Fagiano, and M. Morari, "Real-time optimization and adaptation of the crosswind flight of tethered wings for airborne wind energy," *IEEE Transactions on Control Systems Technology*, vol. 23, no. 2, pp. 434–448, 2014.

[13] U. Fechner and R. Schmehl, "High level control and optimization of kite power systems," in *Proceedings of the 8th PhD Seminar on Wind Energy in Europe, Zurich, Switzerland*, 2012, pp. 12–13.

[14] Altaeros Energies. [Online]. Available: http://www.altaeros.com/

[15] C. E. Rasmussen and C. K. Williams, *Gaussian processes for machine learning*. MIT press Cambridge, MA, 2006.

[16] S. Bin-Karim, A. Bafandeh, A. Baheri, and C. Vermillion, "Spatiotemporal optimization through gaussian process-based model predictive control: A case study in airborne wind energy," *IEEE Transactions on Control Systems Technology*, vol. 27, no. 2, pp. 798–805, 2017.

[17] A. Baheri and C. Vermillion, "Altitude optimization of airborne wind energy systems: A bayesian optimization approach," in *2017 American Control Conference (ACC)*. IEEE, 2017, pp. 1365–1370.

[18] L. N. Dunn, C. Vermillion, F. K. Chow, and S. J. Moura, "On wind speed sensor configurations and altitude control in airborne wind energy systems," in *2019 American Control Conference (ACC)*. IEEE, 2019, pp. 2197–2202.

[19] M. L. Loyd, "Crosswind kite power (for large-scale wind power production)," *Journal of energy*, vol. 4, no. 3, pp. 106–111, 1980.

[20] R. E. Kalman, "A new approach to linear filtering and prediction problems," *Journal of Basic Engineering*, 1960.

[21] N. Wiener, *Extrapolation, interpolation, and smoothing of stationary time series: with engineering applications*. MIT press, 1950.

[22] S. G. Mohinder and P. A. Angus, "Kalman filtering: theory and practice using matlab," *John Wileys and Sons*, 2001.

[23] A. Carron, M. Todescato, R. Carli, L. Schenato, and G. Pillonetto, "Machine learning meets kalman filtering," in *2016 IEEE 55th Conference on Decision and Control (CDC)*. IEEE, 2016, pp. 4594–4599.

[24] J. Reed, M. Cobb, J. Daniels, A. Siddiqui, and C. Vermillion, "Hierarchical control design and performance assessment of an ocean kite in a turbulent flow environment," in *2020 IFAC World Congress*, 2020.

[25] E. F. Camacho and C. B. Alba, *Model predictive control*. Springer Science & Business Media, 2013.

[26] S. Costello, C. Costello, G. François, and D. Bonvin, "Analysis of the maximum efficiency of kite-power systems," *Journal of renewable and sustainable energy*, vol. 7, no. 5, p. 053108, 2015.

[27] C. Archer, "Wind profiler at Cape Henlopen. Lewes, Delaware," 2014.

[28] B. Haydon, J. Cole, L. Dunn, P. Keyantuo, T. Chow, S. Moura, and C. Vermillion, "Empirical regret bounds for control in spatiotemporally varying environments: A case study in airborne wind energy," in *Dynamic Systems and Control Conference*. ASME, 2019.